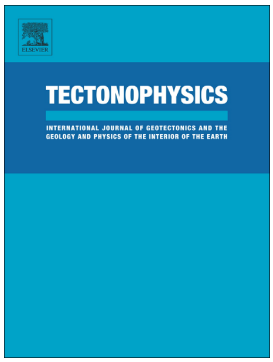

Late Pleistocene acceleration of deformation across the northern Tianshan piedmont (China) evidenced from the morpho-tectonic evolution of the Dushanzi anticline

Julien Charreau, Dimitri Saint-Carlier, Jérôme Lavé, Stéphane Dominguez, Pierre-Henri Blard, Jean-Philippe Avouac, Nathan D. Brown, Luca Claude Malatesta, Wang Shengli, Edward J. Rhodes

PII: S0040-1951(18)30089-1
DOI: doi:10.1016/j.tecto.2018.02.016
Reference: TECTO 127788

To appear in: *Tectonophysics*

Received date: 11 December 2017
Revised date: 21 February 2018
Accepted date: 25 February 2018

Please cite this article as: Julien Charreau, Dimitri Saint-Carlier, Jérôme Lavé, Stéphane Dominguez, Pierre-Henri Blard, Jean-Philippe Avouac, Nathan D. Brown, Luca Claude Malatesta, Wang Shengli, Edward J. Rhodes , Late Pleistocene acceleration of deformation across the northern Tianshan piedmont (China) evidenced from the morpho-tectonic evolution of the Dushanzi anticline. The address for the corresponding author was captured as affiliation for all authors. Please check if appropriate. Tecto(2017), doi:10.1016/j.tecto.2018.02.016

Late Pleistocene acceleration of deformation across the northern Tianshan piedmont (China) evidenced from the morpho-tectonic evolution of the Dushanzi anticline

Julien Charreau[1], Dimitri Saint-Carlier[1], Jérôme Lavé[1], Stéphane Dominguez[2], Pierre-Henri Blard[1], Jean-Philippe Avouac[3], Nathan D. Brown[4], Luca Claude Malatesta[3], Wang Shengli[5] and Edward J. Rhodes [4,6]

1. Centre de Recherche Pétrographique et Géochimique.-, Université de Lorraine - CNRS, , UMR 7358, 15 rue Notre Dame des Pauvres, B.P. 20, 54501 Vandœuvre lès Nancy, France
2. University of Montpellier, Géosciences Montpellier, UMR 5243, Place E. Bataillon, case 060 - 34095 Montpellier Cedex 5, France
3. California Institute of Technology, Division of Geology and Planetary Sciences, 1200 E California Blvd, Pasadena CA 91125, United States
4. University of California, Department of Earth, Planetary and Space Sciences, Los Angeles, California 90095-1567, United States
5. Nanjing University, Department of Earth and Sciences, Nanjing, China
6. Department of Geography, University of Sheffield, Sheffield, S10 2TN, UK

Keys words: tectonic; shortening rates; Dushanzi Kuitun; Tianshan; alluvial terrace; growth-strata; piedmont.

Abstract

We document the temporal evolution of deformation in the northern Tianshan piedmont where the deformation is partitioned across several thrusts and folds. We focus on the Dushanzi anticline, where abandoned terraces and growth strata allow us to constrain the history of folding since the Miocene. Based on subsurface seismic imaging, structural measurements and morphological analysis, we show that this anticline is associated with two decollement levels. We use kink band migration in growth strata dated by paleomagnetism to constrain the shortening from the Mio-Pliocene to the Holocene. Our results show that the Dushanzi anticline has been active since at least 8 Ma and that the fold grew at a steady shortening rate of 0.6±0.1 mm/yr from 8 to ~1.5 Ma with possible variations from 2.5 to 1.5 Ma. Then it accelerated rapidly to a rate of 4.3±1.0mm/yr over at least the last 100 ka. These results, together with similar temporal shortening evolutions across other structures, suggest that the deformation rate across the eastern Tianshan piedmont increased relatively recently. This may reflect either a redistribution of the deformation from the internal structures toward the borders or a general acceleration of the deformation across the entire range.

1/Introduction

The Tianshan is a major mountain range that reaches elevations of over 7000 m and dominates the topography of central Asia. The range laterally extends over a distance >1500 km, with both width and average elevation decreasing from west to east (Fig.1). In more detail, the

topography is composed of a series of elevated ranges (>4000 m) separated by very large E-W striking intermontane basins. The overall range rose during the Oligocene and Miocene in response to the India/Eurasia collision, which reactivated numerous structures originally formed during earlier Paleozoic collision and subduction episodes (Chen et al., 1999; Dumitru et al., 2001; Gao et al., 1998). Geodetic measurements indicate that in its western part the Tianshan accommodates up to 20 mm/yr, i.e. 40% of the total present-day convergence between India and Asia (Abdrakhmatov et al., 1996; Wang et al., 2001; Yang et al., 2008; Zubovich et al., 2010). The present shortening rate decreases eastward, mimicking the lateral variations in topography and width of the range (Reigber *et al.*, 2001; Wang *et al.*, 2001; Yang et al., 2008), as a consequence of the regional clockwise rotation of the southern Tarim block (Avouac et al., 1993; Yang et al., 2008; Zubovich et al., 2010). At the longitude of this study, the Tianshan range absorbs ~8 mm/yr of shortening between the Junggar and the Tarim Basins, which are two large intracontinental and endorheic basins, trapping the sediments shed from the uplifting reliefs. These foreland basins have been affected by intense thin-skin tectonics, with folding, thrusting and thickening occurring along both the northern and southern sides of the range. Pleistocene to Holocene deformation can be documented from the deformation of alluvial fans and river terraces (e.g. Avouac et al., 1993; Molnar et al., 1994). The deep structure and deformation over the late Cenozoic can be documented from seismic profiles and from the exceptional exposure of the stratigraphy (Charreau et al., 2008; Daëron et al., 2007; Lu et al., 2010; Stockmeyer et al., 2017, 2014). The northern piedmont of the eastern Tianshan is therefore a natural laboratory in which to study the temporal evolution of a fold-and-thrust belt. Despite a growing number of studies, large uncertainties remain regarding the exact distribution of the deformation between the numerous structures that comprise the piedmont. To better understand how the Tianshan grew, more quantitative constraints are still needed.

Here, we build on previous studies to document the structure and temporal evolution of deformation across the western part of the northern piedmont (Figs. 1 and 2). At the longitude of our study area, three main folds have been identified and described: (from south to north) the Tuositai anticline, the Dushanzi anticline and the Wusu blind fold (Avouac et al., 1993; Deng et al., 1996; Fu et al., 2003; Li et al., 2010). To the south, the Paleozoic rocks of the high range overthrust these foreland structures via the Frontal Tianshan Thrust (Stockmeyer et al., 2014). We focus our analyses on the Dushanzi anticline because it represents the main active structure at this particular longitude and has likely undergone most of the deformation accommodated across the entire northern Tianshan piedmont (Avouac et al., 1993; Poisson and Avouac, 2004; Teng et al., 1996). This fold is currently deforming the Junggar foreland basin and presents a 15-km long and 5-to-7 km wide topographic expression of 800 to 1000 meters maximum height (Figs. 1 and 2). From analyses of warped fluvial terraces or deformed strata, the shortening across this structure was previously

constrained to between 1 and 3 mm/yr (Avouac et al., 1993; Burchfiel et al., 1999; Molnar et al., 1994). However, at the time of these pioneering studies, the depth geometry of the folds and the ages of both the studied morphological markers and deformed strata were barely known. The ages of the Quaternary formations of the Kuitun valley across this fold are now better constrained (Deng et al., 1996; Malatesta et al., 2017; Poisson and Avouac, 2004), the depositional ages of syn-tectonic sediments have been constrained by magnetostratigraphy from 10.5 Ma to 1 Ma (Charreau et al., 2005), and several new seismic lines revealing the depth structure of the fold have been made available (Chen et al., 2012; He et al., 2005). These new data enable both the short-term and long-term shortening rates absorbed by the Dushanzi anticline to be better estimated, providing new insights into the deformation history of the Northern Tianshan piedmont. In the following, based on additional dating of the Kuitun fluvial terraces and a kinematic model of the southern limb of the Dushanzi anticline, we estimate the recent deformation rates from two folded alluvial terrace treads, and the long-term deformation from analysis and modelling of the growth strata. We then discuss the distribution and evolution of the deformation across the northern Tianshan piedmont as well as the implications for the evolution of the entire range.

2/Morpho-tectonic settings

2.1 Morphology of the Dushanzi area

The morphology of the Dushanzi area (Fig. 2) is characterized by a large alluvial fan, probably deposited during the Pleistocene (Guerit et al., 2015; Jolivet et al., 2014; Poisson and Avouac, 2004; Poisson, 2002) (Fig. 2A). The fan was later entrenched by the Kuitun river during the Holocene (Poisson and Avouac, 2004 and Fig. 2A), giving way to the development of a second fan to the north. The latter remains active, trapping most of the coarse sediments currently shed from the high range by the Kuitun River. The entrenchment has left behind numerous terraces, which can be mapped on both sides of the river (Figs. 2 and 3) (Poisson and Avouac, 2004, Malatesta et al., 2017).

In the upstream part of the section, three main large fill-cut terraces, T11, T10 and T9, can be identified 200 to 300 m above the modern river. These terraces all slope northwards at an angle higher than the present river bed (Fig. 4). Only terrace T10 can be traced across the entire anticline and progressively evolves toward a strath terrace above the fold (Figs. 2B and 3) (Molnar et al., 1994). Another strath terrace (T12) located at higher altitude also crosses the anticline but is not present in the upstream part along T9 to T11 (Figs. 2B and 3) (Molnar et al., 1994). Above the fold it is covered by a thick (~10 m) layer of loess (see Fig. B in the online repository data). The elevation across T10 was measured with sub-centimeter accuracy using a differential GPS (black circles). Molnar et al. (1994) measured the heights of T12 along both the depositional and erosional surface using either a total station theodolite or by triangulation. Both terraces present a convex geometry

that is inconsistent with a graded channel slope, suggesting that they have been folded (Fig. 4) (Molnar et al., 1994). In more detail, both terraces show clear and rapid breaks in slope consistent with scarps due to folding or faulting (Fig. 4 and A). However, while terrace T10 shows two breaks and a constant slope between them, terrace T12 presents a third break in the middle. This break can be seen on both the depositional and erosional surfaces (Molnar et al., 1994) and is therefore of tectonic origin and not due to the late eolian deposits. The depositional and erosional surfaces of T12 have therefore recorded the deformation history of the fold and can be used both to assess the shortening rates. As both T10 and 12 were deformed by the same structure at depth, the discrepancy between the two profiles is not therefore of structural origin. Alternatively, we suggest that the abandonment of surface T12 was likely more complex and diachronic (Fig. A and Molnar et al., 1994).

To the north of this convex-up zone, on both the left and right banks of the valley, the river abandoned four wide and flat terraces that slope northwards (Fig. 2B). Here it can be seen that terrace T10 appears to merge with the Pleistocene fan level.

2.2 Ages constrains of the morphological markers

Several studies have constrained either the depositional or abandonment ages of the numerous alluvial terraces identified across the Kuitun valley (Molnar et al., 1994; Poisson and Avouac, 2004; Malatesta et al., 2017; Fig. 2B). Here, we focus our analyses on T10 and T12 because these are, respectively, the most continuous and highest terraces preserved across the fold and may therefore provide the best and longest records of the deformation.

From in situ cosmogenic ^{10}Be concentrations measured in four surface cobbles, Molnar et al. (1994) constrained the abandonment age of T12 south of the Dushanzi anticline to between 14 and 44 ka. They also sampled four surface cobbles on the same surface tilted in the back limb of the fold, constraining the ages to between 41 and 178ka (Fig. 2). These exposure ages remain however somewhat unconstrained, as in addition to the low number of samples and the wide data dispersion, they do not account for inheritance bias nor surface erosion (see the supplementary information section for a discussion of this critical issue). Moreover, they were obtained 20 years ago, and thus require new calibration updates that we perform in this study (see Fig. 4 and the online repository for the revised ages).

From OSL analyses, Poisson (2002) constrained the deposition of this terrace to 86 ka. However, these analyses were performed using a multi-grain single aliquot approach applied to quartz. To better account for the variable and incomplete bleaching that is highly probable in such a fluvial setting, we carried out single-grain post-infrared infrared-stimulated luminescence (SG p-IR IRSL) dating of K-feldspar grains (e.g. Brown et al., 2015). The sample was taken at the base of a 10-m-thick loess layer that tops terrace T12, 40 cm above the contact between the loess and the alluvial

pebbles of the terrace. After digging 50 cm deep to avoid any potential colluvium contamination from the surface, the loess was sampled in a metallic tube and rapidly shielded with black tape. Three additional loess samples were taken at a distance of 30 cm from the OSL tube for radiogenic element measurements. Details of the sample location, treatment and measurements are given in the online repository data and are similar to those used by Rhodes (2015). The final age obtained after correction for fading is 116.1±14.8 ka. As this dating was performed on the eolian cover that seals the terrace deposit it should be considered a minimum estimate of the terrace abandonment age. Nevertheless, it is to the first order coherent with the revised cosmogenic exposure ages of the four surface cobbles sampled and analyzed by Molnar et al. (1994) on the tilted surface located on the backlimb of the fold (Fig. 4).

The exposure age of T10 was initially constrained to be between 8 and 22 ka using in situ cosmogenic data of five surface cobbles (Molnar et al., 1994). We collected an additional depth profile on this terrace. The analysis of this profile, which accounts for the inheritance bias, shows that T10 was likely abandoned between 6 and 14 ka (see the online repository). Stimulated luminescence-based analyses provide actually tighter constraint on the depositional age of this terrace. From OSL analyses, Poisson and Avouac (2004) constrained the timing of its deposition to between 7 and 11 ka. Malatesta et al. (2017) used SG p-IR IRSL to analyze a new sample collected near the first OSL sampling site (Fig. 2), and revised the depositional age of T10 to 13.4±1.6 ka.

2.3 *Structure of the Dushanzi Anticline*

The detailed structure of the Dushanzi anticline was revealed by the entrenchment of the Kuitun River, a process that exposed continuous outcrops of the folded strata. Bedding attitudes were measured at more than 350 sites along the section and reveal a fairly uniform strike and a change in dip, outlining an anticlinal fold (Figs. 3 and 5). In the northern limb, the south dipping fault reaches the surface and even affects the surface of the young Holocene alluvial fan, as evidenced by a 5-km-long east-west striking fault scarp (Avouac et al., 1993; Deng et al., 1996). Accordingly, the Dushanzi anticline was first described in the literature to be a simple fault bend fold rooted in a single detachment layer that reaches the surface and was recently active (Avouac et al., 1993; Deng et al., 1996; Burchfiel et al., 1999). However, the deep structure revealed by the seismic line is more complicated (see Fig. 5 and the online depository). In the hanging wall of the fault, the deeper reflectors show no significant bed thickness variations and can be assumed parallel to a curved fault ramping up from a subhorizontal décollement at depth. This décollement likely lies in the Jurassic, where numerous levels of coal and clay exist (e.g. BRGMX, 1985; Hendrix et al., 1992). The bedding of these reflectors shows a two-step change in attitude. This suggests the existence of two hinge zones

bounded by four axial surfaces (Fig. 4b). This ramp is probably linked to the major thrust at depth that extends below the range ~15 km to the south (Stockmeyer et al., 2014).

However, this deep décollement cannot be connected to the fault that breaks through at the surface. Moreover, the short wavelength anticline geometry (<2 km) revealed by the surface dip measurements cannot be related to the deep larger scale structure inferred in the seismic line (>5 km). The deep structure of the Dushanzi anticline is not expressed in the actively folded landscape, suggesting that it is no longer active. By contrast, the upper ramp coincides with a fault scarp that is offsetting the river terraces (Figs. 3, 4 and 5). We infer that a décollement at a higher structural level, connected with the active ramp and fault scarp, has more recently been activated, and likely accommodates the present deformation. By analogy with nearby sections (Li et al., 2011; Stockmeyer et al., 2014), this décollement is probably located in the silt rich and lacustrine Anjihai formation of late Paleocene age (BRGMX, 1985; Charreau et al., 2009). Thus, we hypothesize that the thrust follows this formation and parallels the strata along the back limb of the fold (Figs. 5 and 6). Its geometry therefore follows the reflectors at depth and is likely similar to the lower ramp. It likewise includes two step changes in bedding attitude and is rooted in the southern part of the section.

In conclusion, we interpret the geometry of the Dushanzi fold to be a fault-bend-fold anticline with two levels of décollement. In the footwall of this structure, the bedding attitudes are fairly uniform and relatively flat.

3/ Shortening rates across the Dushanzi anticline

3.1/ Kinematic model

The geometry of any layer deformed across a fold can be modelled using a simple geometric formulation of the displacement by assuming that fold growth is controlled by a curved hinge kink-band migration (Suppe et al., 1997). In such a model, the hinge zone has a finite width and is limited by entry and exit axial surfaces (Charreau et al., 2008). The folding and the rotation of the layers are only acquired inside the hinge zone through the hanging wall (Suppe et al., 1997). The geometry of any layer that crosses the hinge zone can be easily computed from a series of equations (See Appendix of Charreau et al., 2008) that rely on the shortening undergone by the modelled strata, S, the radius of curvature of the hinge zone, Rc, and the opening angle of the curved fold, β (Fig. B in the Online depository information). In such a model, the width of the hinge zone is related to the radius of curvature and the opening angle (Fig. E).

In the Dushanzi anticline, this simple model is complicated by the presence of two faults (Fig. 5). The folding of the layers could have therefore resulted from thrusting along one or the other, or both of the two faults. It was likely produced in two steps, first by progressive thrusting on the lower ramp and then by later activation of the upper décollement. However, the bedding and rotation of

the layers were progressively acquired only within the two hinge zones of the two faults as the layers moved forward. Because the seismic reflectors are strictly parallel at depth, the two fault ramps have very similar geometry with similar radius of curvature and opening angle. The rotation experienced by the lower ramp would be equivalent to that on the upper ramp for the same shortening and vice-versa. Therefore, we limited our modelling to the upper fault assuming it represents the cumulative shortening on both ramps equivalent to a scenario that would include deformation on both ramps.

In our model the dip angles of this ramp increases gradually northwards from ~8° to ~30° (Fig. 6) so as to match the dip angles of the seismic reflectors at depth and the dip measurements at the surface. As the location of the fault at the surface is known, only the depth of the décollement was then adjusted to ~2700m at the southern limit of the seismic line. Finally, the width of the hinge zone was set to ~3500m to respect the rapid elevation changes in the topographic terrace profiles of T10 and T12 (Fig. 4). Indeed, these topographic changes should correspond to fold scarps that reveal the location of the hinge zone at the surface (Figs. 4 and A). The radius of curvature (Rc) derived from this setting is ~9170m. Our modelled upper ramp reproduces the deep reflectors well, respecting their curvature at depth as well as the surface topography (i.e. the terraces) (Fig. 6).

3.2 Long term deformation rates

To constrain the deformation rate over a longer time scale, we first modelled the strata present at depth. However, the quality of the seismic data in the upper part is poor, showing only a few reflectors. The modelled strata were therefore compared to the bedding measured at the surface only. These measurements represent the finite result of the shortening on both ramps. To avoid the short wavelength dip variations likely due to measuring biases, we smoothed the data using a 3rd degree polynomial fit. We considered only the southern limb of the Dushanzi anticline where the bedding attitudes decrease progressively. In the northern part, the structure reflects an earlier phase of fault-tip folding, as inferred from comparison with analog experiments (Bernard et al., 2007), which is not modeled here. The shortening of each of the modelled layers was then adjusted to minimize the misfit between the smoothed dip angles at the surfaces and the modelled dip angles (Fig. 6). To derive the history of shortening (Fig. 6), the stratigraphic ages of the modelled horizons were constrained from their horizontal positions along the present river, where the strata have been dated by magnetostratigraphy to be 10.5 to 1.3 My in age (Charreau et al., 2005). Our results suggest continuous and relatively steady fold growth from 8 Ma to ~2.5Ma , with an overall average shortening rate of ~0.6±0.1 mm/yr (Fig. 6B). A possible increase of the deformation between 2.5 and 1.5 followed by a slowdown since 1.5 Ma are also possible, but are attached to large uncertainties.

3.3 Pleistocene shortening rates from warped terrace treads

Based on the same calculations of the displacement and geometry of the upper ramp, we modelled the warped T12 and T10 terrace treads (Fig. 4). In this case, the modelled terraces will depend on the shortening they have undergone and their initial geometry prior to deformation. The latter should mimic the graded long profile of the river system that created the geomorphic markers. Thus, similar to the present river, we assume that the elevation change of the initial terraces might be approximated by a linear or smoothly evolving profile (Fig. 4). This can be defined using the marker geometry in zones that underwent only uplift and translation but no rotation, unlike in the hinge area (*e.g.* Molnar *et al.*, 1994). The initial slope of terrace T10 before its deformation was thus defined by a linear profile from the DGPS data in the zone uplifted above the steepest part of the ramp, located north of the hinge zone (abscissa ~4000 m to ~6500 m). In contrast, the initial slope of terrace T12 was defined in the southern part of the profile, south of the hinge zone (abscissa ~-2000 m to ~0 m).

Terrace T10 shows only two breaks in slope that are consistent with the structure at depth. This surface must have been abandoned and then deformed without sediment aggradation in the back limb (Fig. 4 and A). The original position of the terrace was therefore restored by a simple translation that depends on the shortening S. The original profile was then deformed across the entire ramp according to the same shortening and using our kink band migration model to fit it to the elevation data of the terrace. Based on a least square adjustment, we found that a shortening of ~57 m yields an overall modelled profile shape that is relatively consistent with the elevation change of the terrace (Fig. 4).

The modelling of terrace T12 was complicated by the presence of the third break in slope located within the hinge zone. This likely reflects diachronism at the surface due to a phase of sediment aggradation in the back limb of the fold, followed by incision and abandonment (Molnar et al., 1994, Fig. A). Therefore, following the Molnar et al. (1994) scenario, and based on our new p-IR IRSL dating results, we assumed that the surface was first abandoned and uplifted at ~116 ka north of the hinge zone. Within and south of the hinge zone, this surface remained partially buried at first due to sediment aggradation as the Pleistocene fan grew. The entire surface was then abandoned because aggradation had stopped and incision started, or at least because the sedimentation was insufficient to compensate for uplift. The total shortening S, the sediment aggradation rate a_r and the time when aggradation stopped t_{ab} were then adjusted to fit to the elevation data by minimizing the Mean Square Deviation (MSD) (Fig. 4). We obtained values of 518 m, 26 ka and 0.7 mm/yr for S, t_b and a_r, respectively. However, a_r and t_b remain first-order estimates and should be treated with caution as we assumed in our scenario that the aggradation was continuous and steady while it is possible that it varied over time. However, our abandonment age remains broadly consistent with

the revised exposure age of the surface cobbles sampled and analysed by Molnar et al. (1994) (Fig. 4). The total shortening value is more robust because it relies only on the steepest part of the profile. This area represents the original abandoned surface and has recorded the full shortening and rotation within the hinge zone.

For both terraces, we attach a large conservative uncertainty of 20% to our shortening values to account for the late loess deposits on T12 and possible errors in the seismic line location and its projection with respect to the terrace profile. Based on the terrace ages of 116.1±14.8 ka (this study) and 13.4±1.6 ka (Malatesta et al., 2017), the shortening rates for T12 and T10 are 4.5±1.0 mm/yr and 4.2±1.0 mm/yr, respectively.

4/Discussion

4.1 Depth structures and folding mechanism

Our interpretation of the depth structure and the associated kinematic model must be questioned to ensure the robustness of our results. A simple explanation of how this structure formed is that the shallower thrust followed a weak structural level that had already been folded due to slip along the deeper thrust fault. This interpretation is quite consistent with the cross-sections of He et al., (2005) and Lu et al., (2007) both of which were derived from parallel seismic profiles nearby. Moreover, two levels of décollement are similarly described in a number of other anticlines in this piedmont as well as in the southern piedmont (e.g. He et al., 2005; Charreau et al., 2008; Guan et al., 2009; Li et al., 2011, Stockmeyer et al., 2014). In accordance with the terrace geometry, we also assumed that the shortening first started on the lower Jurassic detachment and then shifted to the upper late Paleocene décollement. This is also consistent with the structural evolution proposed by He et al. (2005) for the same anticline.

However, while the general kinematics of our fold model are consistent with the literature and other structures in the region, the displacement formulation used is simplistic and the related assumptions might therefore be questioned. We note for example that the few reflectors observed at shallow depth show dip higher than the modelled strata (Fig. 6a). However, this discrepancy is likely due to the velocity-time data used to migrate the profile. Indeed, in this part of the section the strata mainly comprise the coarse conglomeratic Xiyu formation where the seismic velocity is likely higher than the profile average velocity used for the migration. Consequently, the reflectors were flattened during the migration. It is, however, difficult to account for the observed lateral variation of the velocity. More importantly, a significant portion of the strata dip angle may have been acquired by limb rotation and not only through hinge translation. All of the terraces show a gentle northward slope slightly higher than that of the present river bed, while significant limb rotation should have tilted these surfaces southward. This suggests that the impact of limb rotation was limited during the

more recent evolution of the fold (i.e. <100 ka). However, the question remains open at longer timescales, especially at the time when the deformation started and when the fold nucleated, probably as a detachment fold. Not considering a possible rotation would lead to the overestimation of the long term shortening rate, which is already lower than the Pleistocene rate. Likewise, the differential compaction of growth strata might tend to increase the dip angle of the strata and hence have had a similar effect. In a study across the nearby Huerguosi anticline, Charreau et al. (2008) showed that the impact of compaction is probably insignificant compared to the other, larger, uncertainties, especially those associated with the dip angle measurements.

4.2 Deformation rate variations in the Tianshan piedmonts

The strong acceleration observed during the Pleistocene is quite robust but the evidence for the acceleration between 2.5 and 1.5 Ma and the slow down between 1.5 and 116 ka period might seem weak, because in this part of the section, the lithology is composed of the thick, coarse-conglomerate Xiyu formation, in which precise estimation of the bedding attitude is difficult. Our dip measurements, and thus also our derived shortening rates, are therefore associated with a large uncertainty in this particular zone. However, we note that the 5° (0.08 radians) dip angle of the 1.5 Ma old growth strata at the top of the magnetostratigraphic section requires a shortening of no more than 800 m (Rc x 0.08 radians) since their deposition. Given that terrace T12 requires 518 m of shortening over the last 116 ka, only about 30 0m of shortening is expected to have accrued between 1.5 Ma and 116 ka. This corresponds to an average rate of only 0.2 mm/yr. We conclude that a prolonged period of slow shortening must have occurred between 1.5 Ma and 116 ka. This deceleration would imply that during this period of time, part of the shortening accommodated across the Dushanzi anticline was absorbed across other structures, either more frontal, such as the Wusu anticline, or located further back, such as the Tutsoi anticline (Figs. 1 and 5).

The deformation history of the Dushanzi anticline can be compared to the shortening recorded across other folds on the piedmont. In the Anjihai anticline, located 50 km along strike to the west (Fig. 1), Daëron et al., (2007) estimated from fold modelling that the deformation across this detachment fold started at 7.4 Ma at a shortening rate of 0.4 mm/yr and continued at this rate until 0.9 Ma, when it accelerated to 1.12 mm/yr. From analysis of a folded terrace, Fu et al. (2017) found that the same anticline shortened at a rate of 0.4-0.7 mm/yr between 53 ka and 9 ka and at a rate of 1.1-1.4 mm/yr since 9 ka. Even if the exact timing may differ, the variations of the deformation rates are relatively similar across both folds. The deformation remains weaker in the Anjihai anticline. This is likely linked to the growth of the Huerguosi anticline located to the south of the Anjihai (Fig. 1). This fault-bend fold was also active during this period of time, accommodating 0.84 mm/yr and 1.14 mm/yr of shortening, from 10 to 4 Ma and from 4 Ma to present, respectively (Charreau et al., 2008).

Since the Anjihai and Huerguosi anticlines are parallel and are located at the same longitude, their deformations can be summed. This yields a total shortening of ~1.2 mm/yr, which progressively accelerated to ~2.3 mm/yr. These values are lower than our own estimates across the Dushanzi anticline. The difference between the two sections may reflect the existence of active structures south of the Huerguosi anticline. The South Anjihai and South Tugulu anticlines may extend laterally south of the Huerguosi anticline and accommodate a part of the deformation (Fig. 1). Similarly, the main thrust located at the front of the Paleozoic range may have also been active during the period (Fig. 1). In the Tugulu anticline, located ~100 km east of our study area (Fig. 1), Stockmeyer et al. (2017) reported deformation rates that decrease from ~4 to ~1 mm/yr at the Holocene transition based on folded terraces. However, the Neogene rates remain unknown across this fold.

Despite these results suggesting a deceleration, several other recent studies across folds located in the southern Tianshan piedmont at the same longitude suggest an acceleration of deformation during the last ~1 Myr (Heermance et al., 2008; Hubert-Ferrari et al., 2007; Saint-Carlier et al., 2016). The total deformation across this piedmont and the evolution of this deformation though time have not yet been accurately constrained. Taken together, the existing data suggest a 3- to 4-fold increase in the deformation rates within the Tianshan piedmonts sometime between the Neogene and the Pleistocene (Fu et al., 2017). More studies are needed to unambiguously confirm this acceleration, and our conclusion must be therefore handled with caution. However if it proves correct, the acceleration may have several origins.

It may reflect a redistribution of the deformation from the inner toward the more external structures of the orogen. Indeed, Mio-Pliocene sediment progradation rates measured across the two piedmonts suggest that the long term deformation rates across the entire range were ~6 mm/yr (Charreau et al., 2009). This is a crude estimate but it remains similar to the present shortening rate derived from GPS of ~8.5 mm/yr across the range (Yang et al., 2008). If we assume that the deformation rates were balanced in the long term and remained constant during the Neogene at a value similar to the present, then <10% of this total crustal deformation would have been initially accommodated within the northern Tianshan piedmont. Since the Holocene, the value would have increased to up to ~50%. At this longitude, a significant part (>15 %) of the total present crustal shortening across the range is accommodated in the internal part the range (Charreau et al., 2017). Accordingly, the Eastern Central Tianshan is thickening at a rate that is significantly faster/higher than the average denudation rates (Charreau et al., 2017), suggesting that the Tianshan range has not yet reached a steady topography and remains in a transient state of growth. Such acceleration and redistribution of the deformation toward the piedmont may suggest evolution of the orogen toward a more steady topography in which deformation is progressively being focused at the

borders, as observed in other large and more mature orogenic belts such as in the Himalayas (Lavé and Avouac, 2001). Such a redistribution of the deformation may be also forced by sedimentation-tectonic interactions within the piedmont. Indeed, syn-tectonic sedimentation across an active fold may overload the fault, increase the shear stress and influence the geometry and kinematics of the folding (Barrier et al., 2013; Fillon et al., 2013; Mugnier et al., 1997). In situ cosmogenic measurement on sediments reveal strong variations in paleo-denudation rates of the Kuitun river drainage basin between 3 and 1.5 Ma (Puchol et al., 2017). These results suggest that the sediment fluxes delivered to the foreland basin also rapidly varied during this time. However, these data are attached to too large uncertainties to unambiguously link these change to the deformation rate history across the Dushanzi anticline. We also cannot exclude the alternative interpretation of a general acceleration of the deformation across the entire range. However, the convergence between India and Asia (~45 mm/yr) (Patriat and Achache, 1984) and the deformation accommodated across the Himalaya (~20 mm/yr) (Lyon-Caen and Molnar, 1985) have both remained relatively steady during the Miocene. Therefore, if the deformation across the whole Tianshan has recently increased during the Quaternary it would require a diminishing deformation accommodated within the Tibet and especially across the Kunlun Mountains and the Atltyn Tagh fault that bound the plateau to the North. To our knowledge there is no evidence yet for such a large-scale geodynamic reorganisation.

Conclusions

In the Kuitun section, surface geology and morphology as well as seismic imaging at depth reveal a fault-bend-fold system which involves two thrust faults. Only the upper structure has actively deformed the landscape. Several alluvial terraces were deposited, abandoned and subsequently deformed across this fold. Though somewhat loose and associated with large uncertainties, our CRN surface exposure dating of the main terrace, T10, suggests this surface was abandoned between 6 and 15 kyr, in agreement with the previous luminescence age of 13.6 ka of Malatesta et al. (2017). We also provide a new p-IR IRSL age for the upper terrace, T12, which constrains its abandonment age to 116.1±14.8 kyr.

Based on a simple geometric formulation of the displacement, we modelled both the pre-growth strata and the growth strata, integrating the geometry of these two deformed and dated alluvial terraces. This work highlights the presence of growth strata on the Dushanzi fold since at least 9 Ma. We also propose that the Dushanzi anticline has shortened at an average rate of ~0.6 mm/yr since at least ~8 Ma, with possible periods of acceleration and deceleration for the last 2.5 Ma. This rate recently (between 116ka and ~1.5 Ma?) increased to ~4 mm/yr. While this method can be applied to complex and mature structures such as the Dushanzi anticline, it neglects the possible rotation mechanism and may therefore overestimate the deformation rates. Investigation of the

temporal evolution of folding and thrusting of other structures in the northern and southern Tianshan piedmont will help determine if the temporal variations in deformation are due to local interactions between neighbouring structures or to a regional evolution that could be related to the effects of climate-driven erosion and sedimentation, purely tectonic processes, or geodynamics at the regional scale.

Acknowledgements

This study was financed by the French INSU/CNRS SYSTER program. We are grateful to the ASTER team for the cosmogenic nuclide concentration measurements (M. Arnold, G. Aumaître, K. Keddadouche, L. Léanni and F. Chauvet). The ASTER national AMS facility (CEREGE, Aix en Provence) is supported by the INSU/CNRS, the French Ministry of Research and Higher Education, IRD and CEA. We also thank Richard Heermance and Aurelia Hubert-Ferrari for their reading and contribution to the improvement of this manuscript. This is CRPG contribution n° 2565.

Bibliography

Abdrakhmatov, K.Y., Aldazhanov, S.A., Hager, B.H., Hamburger, M.W., Herring, T.A., Kalabaev, K.B., Makarov, V.I., Molnar, P., Panasyuk, S. V, Prilepin, M.T., Reilinger, R.E., Sadybakasov, I.S., Souter, B.J., Trapeznikov, Y.A., Tsurkov, V.Y., Zubovich, A. V, 1996. Relatively recent construction of the Tien Shan inferred from GPS measurements crustal deformation rates. Nature 384, 450–453.

Avouac, J.P., Tapponnier, P., Bai, M., You, H., Wang, G., 1993. Active Thrusting and Folding Along the Northern Tien-Shan and Late Cenozoic Rotation of the Tarim Relative to Dzungaria and Kazakhstan. J. Geophys. Res. Earth 98, 6755–6804. doi:Doi 10.1029/92jb01963

Barrier, L., Nalpas, T., Gapais, D., Proust, J., 2013. Impact of synkinematic sedimentation on the geometry and dynamics of compressive growth structures : Insights from analogue modelling. Tectonophysics 608, 737–752. doi:10.1016/j.tecto.2013.08.005

Bernard, S., Avouac, J.P., Dominguez, S., Simoes, M., 2007. Kinematics of fault-related folding derived from sandbox experiment. J. Geophys. Res. 112, doi:10.129/2005JB0044149.

BRGMX, 1985. Geological map of the Xinjiang Uygur Autonomous Region, China. China Geol. Print. House.

Brown, N.D., Rhodes, E.J., Antinao, J.L., Mcdonald, E. V, 2015. Single-grain post-IR IRSL signals of K-feldspars from alluvial fan deposits in Baja California Sur , Mexico. Quat. Int. 362, 132–138. doi:10.1016/j.quaint.2014.10.024

Burchfiel, B.C., Brown, E.T., Deng, Q., Li, J., Feng, X., Molnar, P., Shi, J., Wu, Z., You, H., 1999. Crustal

Shortening on the Margins of the Tian Shan, Xinjiang, China. Int. Geol. Rev. 41, 663–700.

Charreau, J., Avouac, J.-P., Chen, Y., Dominguez, S., Gilder, S., 2008. Miocene to present kinematics of fault-bend folding across the Huerguosi anticline, northern Tianshan (China), derived from structural, seismic, and magnetostratigraphic data. Geology 36, 871–874. doi:10.1130/G25073A.1

Charreau, J., Chen, Y., Gilder, S., Dominguez, S., Avouac, J.-P., Sen, S., Sun, D., Li, Y., Wang, W.M., 2005. Magnetostratigraphy and rock magnetism of the Neogene Kuitun He section (northwest China): Implications for Late Cenozoic uplift of the Tianshan mountains. Earth Planet. Sci. Lett. 230, 177–192. doi:10.1016/j.epsl.2004.11.002

Charreau, J., Gumiaux, C., Avouac, J.-P., Augier, R., Chen, Y., Barrier, L., Gilder, S., Dominguez, S., Charles, N., Wang, Q., 2009. The Neogene Xiyu Formation, a diachronous prograding gravel wedge at front of the Tianshan: Climatic and tectonic implications. Earth Planet. Sci. Lett. 287, 298–310. doi:10.1016/j.epsl.2009.07.035

Charreau, J., Saint-Carlier, D., Dominguez, S., Lavé, J., Blard, P.-H., Avouac, J.-P., Jolivet, M., Chen, Y., ShengLi, W., Borwn, N.D., Malatesta, L.C., Rhodes, E., Team, A., 2017. Denudation outpaced by crustal thickening in the eastern Tianshan. Earth Planet. Sci. Lett. 479, 179–191.

Chen, C., Lu, H., Jia, D., Cai, D., Wu, S., 1999. Closing history of the southern Tianshan oceanic basin, western China: an oblique collisional orogeny. Tectonophysics 302, 23–40.

Chen, W., Hao, J.J., Li, S.Q., Peng, W.L., Xian, D., Chen, L.H., Li, Z.G., 2012. The geometric and kinematic numerical simulation of the Dushanzi anticline, southern Junggar Basin. Chinese J. Geol. 47, 37–50.

Daëron, M., Avouac, J.-P., Charreau, J., 2007. Modeling the shortening history of a fault tip fold using structural and geomorphic records of deformation. J. Geophys. Res. 112, B03S13. doi:10.1029/2006JB004460

Deng, Q., Zhang, P., Xu, X., Yang, X., Peng, S., Feng, X., 1996. Paleosismology of the northern piedmont of Tianshan Moutains, northwesr China. J. Geophys. Res. 101, 5895–5920.

Dumitru, T.A., Zhou, D., Chang, E.Z., Graham, S.A., Hendrix, M.S., Sobel, E.R., Caroll, A.R., 2001. Uplift, exhumation, and deformation in the Chinese Tian Shan, in: Hendrix, M.S., Davis, G.A. (Eds.), Paleozoic and Mesozoic Tectonic Evolution of Central Asia : From Continental Assembly to Intracontinental Deformation. Geological Society of America Memoir 194, Boulder : colorado, pp. 71–99.

Fillon, C., Huismans, R.S., van der Beek, P., 2013. Syntectonic sedimentation effects on the growth of fold-and-thrust belts. Geology 41, 83–86. doi:10.1130/G33531.1

Fu, B., Lin, A., Kano, K., Maruyama, T., Guo, J., 2003. Quaternary folding of the eastern Tian Shan, northwest China. Tectonophysics 369, 79–101.

Fu, X., Li, S., Li, B., Fu, B., 2017. A fluvial terrace record of late Quaternary folding rate of the Anjihai anticline in the northern piedmont of Tian Shan , China. Geomorphology 278, 91–104. doi:10.1016/j.geomorph.2016.10.034

Gao, J., Li, M., Xiao, X., Tang, Y., He, G., 1998. Paleozoic tectonic evolution of the Tianshan Orogen, northwestern China. Tectonophysics 287, 213–231.

Guerit, L., Barrier, L., Jolivet, M., Fu, B., Métivier, F., 2015. Denudation intensity and control in the Chinese Tian Shan: new constraints from mass balance on catchment-alluvial fan systems. Earth Surf. Process. Landforms n/a–n/a. doi:10.1002/esp.3890

He, D., Suppe, J., Geng, Y., Shuwei, G., Shaoying, H., Xin, S., Xiaobo, W., Chaojun, Z., 2005. Guide book for field trip in south and north Tianshan foreland basin, Xinjiang Uygur Autonomous Region, China, in: International Conference on Theory and Application of Fault-Related Folding in Foreland Basins. Beijing, p. 77.

Heermance, R. V, Chen, J., Burbank, D.W., Miao, J., 2008. Temporal constraints and pulsed Late Cenozoic deformation during the structural disruption of the active Kashi foreland , northwest China 27, 1–27. doi:10.1029/2007TC002226

Hendrix, M.S., Graham, A.S., Carroll, A.R., Sobel, E.R., McKnight, C.L., Schulein, B.J., Wang, Z., 1992. Sedimentary record and climatic implications of deformation in the Tian Shan : Evidence from Mesozoic strata of the north Tarim, south Junggar, and Turpan Basins, northwest China. Geol. Soc. Am. Bull. 104, 53–79.

Hubert-Ferrari, A., Suppe, J., Gonzalez-Mieres, R., Wang, X., 2007. Mechanism of active folding of the landscape (southern Tianshan, China). J. Geophys. Res. 112, doi: 10.129/2006JB004362.

Jolivet, M., Barrier, L., Dominguez, S., Guerit, L., Heilbronn, G., Fu, B., 2014. Unbalanced sediment budgets in the catchment-alluvial fan system of the Kuitun River (northern Tian Shan, China): Implications for mass-balance estimates, denudation and sedimentation rates in orogenic systems. Geomorphology 214, 168–182. doi:10.1016/j.geomorph.2014.01.024

Lavé, J., Avouac, J.P., 2001. Fluvial incision and tectonic uplift across the Himalayas of central Nepal. J. Geophys. Res. 106, 26561. doi:10.1029/2001JB000359

Li, C., Guo, Z., Dupont-nivet, G., 2011. Cenozoic tectonic deformation across the northern foreland of the Chinese Tian Shan. J. Asian Earth Sci. 42, 1066–1073. doi:10.1016/j.jseaes.2010.08.009

Li, C., Guo, Z., Dupont-nivet, G., 2010. Late Cenozoic tectonic deformation across the northern foreland of the Chinese Tian Shan. J. ASIAN EARTH Sci. doi:10.1016/j.jseaes.2010.08.009

Lu, H., Burbank, D.W., Li, Y., 2010. Alluvial sequence in the north piedmont of the Chinese Tian Shan over the past 550 kyr and its relationship to climate change. Palaeogeogr. Palaeoclimatol. Palaeoecol. 285, 343–353. doi:10.1016/j.palaeo.2009.11.031

Lyon-Caen, H., Molnar, P., 1985. Gravity anomalies, flexure of the Indian plate and the structure,

support and evolution of the Himalaya and Ganga basin. Tectonics 4, 513–538.

Malatesta, L.C., Avouac, Jean-Philippe Brown, N.D., Breitenbach, S.F.M., Pan, J., Chevalier, M.-L., Rhodes, E., Saint-Carlier, Dimitri Zhang, W., Charreau, J., Lavé, J., Blard, P.-H., 2017. Lag and mixing during sediment transfer across the Tian Shan piedmont caused by climate-driven aggradation-incision cycles. Bull. Geol. Soc. Am. In press.

Molnar, P., Brown, E.T., Burchfiel, B.C., Deng, Q., Feng, X., Li, J., Raisbeck, G.M., Shi, J., Wu, Z., Yiou, F., You, H., 1994. Quaternary Climate Change and the Formation of River Terraces across Growing Anticlines on the North Flank of the Tianshan, China. J. Geol. 102, 583–602.

Mugnier, J.L., Baby, P., Français, I., Préau, D.B., Géodynamique, L. De, Gignoux, M., Bale, P., Français, I., Préau, D.B., 1997. Thrust geometry controlled by erosion and sedimentation : A view from analogue models 427–430.

Patriat, P.A., Achache, J., 1984. India-Eurasia collision chronology has implications for crustal shortening and driving mechanisms of plates. Nature 311, 615–621.

Poisson, B., 2002. Impact du climat et de la tectonique sur l'évolution géomorphologique d'un piémont : exemple du piémont Nord du Tian Shan depuis la fin du Pléistocène. University of Paris XI, Paris.

Poisson, B., Avouac, J.P., 2004. Holocene hydrological changes inferred from alluvial stream entrenchment in North Tian Shan (Northwestern China). J. Geol. 112, 231–249.

Puchol, N., Charreau, J., Blard, P., Lavé, J., Dominguez, S., Pik, R., Saint-carlier, D., ASTER Team, 2017. Limited impact of Quaternary glaciations on denudation rates in central Asia. Geol. Soc. Am. Bull. 129, 479–499.

Rhodes, E.J., 2015. Dating sediments using potassium feldspar single-grain IRSL : Initial methodological considerations. Quat. Int. 362, 14–22. doi:10.1016/j.quaint.2014.12.012

Saint-Carlier, D., Charreau, J., Lavé, J., Blard, P.H., Dominguez, S., Avouac, J.-P., Wang, S., Arnold, M., Aumaître, G., Keddadouche, K., Léanni, L., Chauvet, F., Bourlés, D.L., 2016. Major temporal variations in shortening rate absorbed along a large active fold of the southeastern Tianshan piedmont (China). Earth Planet. Sci. Lett. 434, 333–348. doi:10.1016/j.epsl.2015.11.041

Stockmeyer, J.M., Shaw, J.H., Brown, N.D., Rhodes, E.J., Richardson, P.W., Wang, M., Lavin, L.C., Guan, S., Sciences, S., Angeles, C.L., Young, C., East, D., 2017. Active thrust sheet deformation over multiple rupture cycles : A quantitative basis for relating terrace folds to fault slip rates. Geol. Soc. Am. Bull. 1–20. doi:10.1130/B31590.1

Stockmeyer, J.M., Shaw, J.H., Guan, S., 2014. Seismic Hazards of Multisegment Thrust-Fault Ruptures: Insights from the 1906 Mw 7.4-8.2 Manas, China, Earthquake. Seismol. Res. Lett. 85, 801–808. doi:10.1785/0220140026

Suppe, J., Sabat, F., Munoz, J.A., Poblet, J., Roca, E., Verges, J., 1997. Bed-by-bed fold growth by kink-

band migration; Sant Llorenc de Morunys, eastern Pyrenees. J. Struct. Geol. 19, 443–461.

Teng, Z.H., Yue, L.P., Pu, R.H., Deng, X.Q., Bian, X.W., 1996. The magnetostratigraphic age of the Xiyu Formation. Geol. Rev. 42, 481–489.

Wang, Q., Zhang, P.-Z., Freymueller, J.T., Bilham, R., Larson, K.M., Lai, X., You, X.Z., Niu, Z.J., Wu, J.C., Li, Y.X., Liu, J.N., Yang, Z.Q., Chen, Q.Z., 2001. Present-day crustal deformation in China constrained by global positioning system measurements. Science (80-.). 294, 574–577.

Yang, S., Jie, L.I., Qi, W., 2008. The deformation pattern and fault rate in the Tianshan Mountains inferred from GPS observations. Sci. China Ser. D-Earth Sci. 51, 1064–1080. doi:10.1007/s11430-008-0090-8

Zubovich, A. V, Wang, X., Scherba, Y.G., Schelochkov, G.G., Reilinger, R., Reigber, C., Mosienko, O.I., Molnar, P., Michajljow, W., Makarov, V.I., Li, J., Kuzikov, S.I., Herring, T.A., Hamburger, M.W., Hager, B.H., Dang, Y., Bragin, V.D., Beisenbaev, R.T., 2010. GPS velocity field for the Tien Shan and surrounding regions 29, 1–23. doi:10.1029/2010TC002772

Table and figure captions

Figure 1: A: Shaded SRTM topography of Central Asia with GPS horizontal velocity (Yang et al., 2008). B: Satellite map of the northern Tianshan foreland showing locations of earthquakes recorded since 1930 (USGS ANSS catalog). Note in particular the recent 5.2 magnitude earthquake that shook this area on 22 February 2015, highlighting the active deformation in the region. The dashed box indicates the location of our studied area.

Figure 2: A: Geomorphologic and tectonic map of the Dushanzi area, showing the two imbricate fans and the location of the Dushanzi anticline. B: Spot DEM shaded topography showing the locations of the main alluvial terraces identified (T12 to T7). Their identification and mapping (Fig. 2B) were based on Malatesta et al. (2017), who interpreted the terrace morphology from detailed Lidar measurements. Because terrace T12 is constituted by only few relics it cannot be mapped precisely. Its extension and location can be seen from the purple crosses which represent the location of the theodolite survey made by Molnar et al. (1994). The different age data and their associated methods are reported in the white boxes. The surface 10Be cobble ages of Molnar et al. (1994) were revised using new calibration updates. These ages were not corrected for the inherited concentration derived from the cosmogenic profile inversion (Online repository). The exact locations of the four cobbles sampled by Molnar et al. (1994) in their southern section on the upper terrace T12 remain unknown. The dashed line indicates the projection line used to plot the topographic profile in Figure 4. The zero distance corresponds to the southern limit of the seismic profile.

Figure 3: Panorama of the Dushanzi Anticline and its morpho-structural interpretation (bottom). The colors indicate the different terraces levels with darker color showing the sediments and lighter colors the terraces surfaces. The terrace T3 is one of the lower surfaces that were mapped as "T7 and lower" in figure 2.

Figure 4: Topographic profiles of terraces T10 and T12. The profile for T12 includes the point measured using a theodolite (Figure 2) but also the heights measured by triangulation. Both profiles were corrected for the slope of the original abandoned surface (dashed red lines) in order to quantify the uplift they have recorded. The red lines show our best-fitting model and associated shortening estimates. For T10 we also show in light blue and orange two other surfaces modelled using different values of shortening. For T12 the dashed blue line indicates the geometry of the surface without sediment aggradation. The surface cobble ages were calculated from the data of Molnar et al. (1994) and revised using new calibration updates. These ages were not corrected for the inherited concentration derived from the profile inversion (Online repository). The inset diagrams show the parameters tested (S, a_r and t_{ab}) against the residual square of the mean. S is the total shortening, a_r the sediment aggradation rate and t_{ab} the time when aggradation stopped. We estimated the difference between the elevation of each point of the measured profiles and the modelled heights at the same horizontal coordinate. Then, based on all these difference we calculated the residual square of mean (MSD). Lower MSD values imply a better model fit.

Figure 5: Simplified cross section of the Northern Tianshan piedmont at the longitude of the Dushanzi anticline with a line drawing of the seismic profile provided by Chen et al. (2012). The structure of the Dushanzi anticline was constrained from seismic subsurface imaging and surface structural measurements. Measured dip angles along the Kuitun River are shown as green segments while the main seismic reflectors are shown in gray. The orange line indicates the axial surface used in our fold model.

Figure 6: A: Pre-growth and growth strata predicted by our model using the surface bedding dip adjustment method and comparison with the seismic line drawing (only half of the lines were drawn; see figure D in the online appendix for a complete view). B: Measured (green circle), smoothed (red line) and modelled (blue circle) dip angles against the horizontal distance along the section. C: temporal evolution of the shortening rates across the Dushanzi anticline for each of the modelled layers. Assuming 5° for the 1σ uncertainty in each individual dip angle measurement, we used the Chi-square criterion to estimate the resulting uncertainty in shortening at the 67% (1σ) confidence level. This uncertainty accounts for measurement errors and for the natural roughness of bedding surfaces. Each age is assigned to a confidence interval corresponding to the chron defined by the magnetostratigraphic data points that bracket the stratigraphic location of the point of interest. However, for each point we assumed a symmetrical uncertainty using the maximum limit.

Following the approach developed by York et al. (2004), the average shortening rate and its uncertainty was constrained using a general least-squares procedure that allows the uncertainties in the shortening estimates as well as in the ages to be taken into account. The inset diagram shows the shortening versus time as derived from the modelling of the two warped terraces (see Fig. 4).

Research highlights

"Late Pleistocene acceleration of deformation across the northern Tianshan piedmont (China) evidenced from the morpho-tectonic evolution of the Dushanzi anticline" (TECT012453)

- We document the temporal evolution of deformation across the Dushanzi anticline.
- The history of folding is constrained based on the modeling of growth strata
- The Dushanzi anticline has been active since at least 8 Ma at a rate of 0.6±0.1 mm/yr
- It accelerated rapidly to a rate of 4.3±1.0mm/yr over at least the last 100 ka.
- Deformation rate across the eastern Tianshan piedmont likely increased recently.

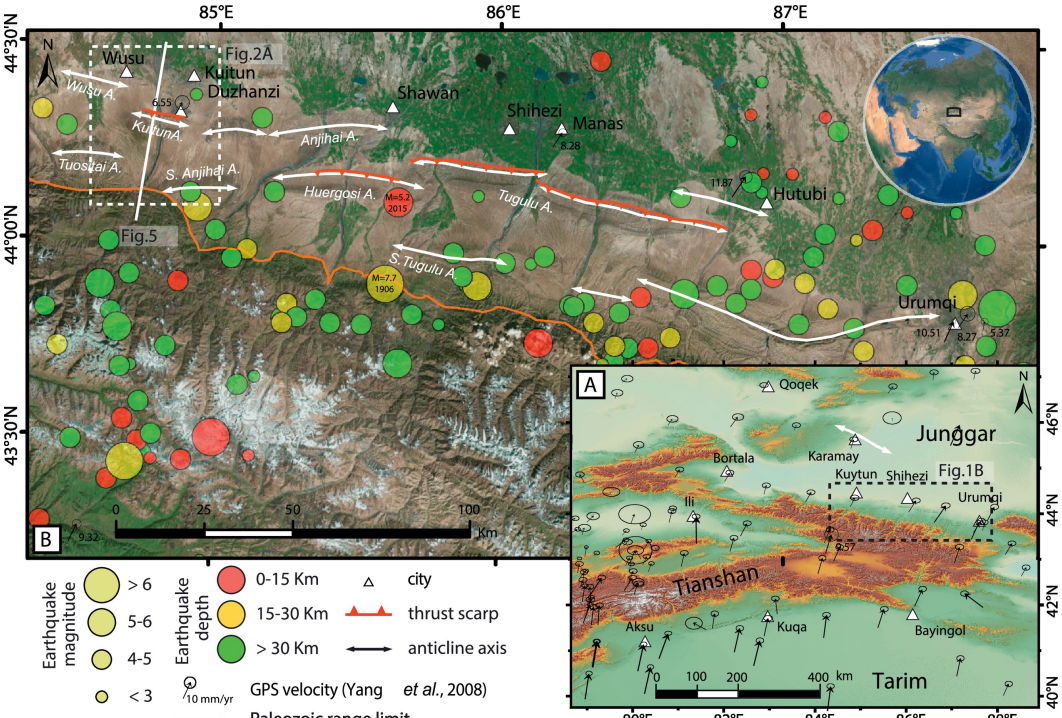
85°E
86°E
87°E
44°30'N
44°00'N
43°30'N
N
Wusu
Kuitun
Duzhanzi
Fig.2A
Fig.5
Shawan
Shihezi
Manas
Hutubi
Urumqi
Wusu A.
KuitunA.
Anjihai A.
Tuositai A.
S. Anjihai A.
Huergosi A.
Tugulu A.
S. Tugulu A.
M=5.2
2015
M=7.7
1906
6.55
8.28
11.87
10.51
8.27
5.37
9.32
0
25
50
100
km
B
A
Qoqek
Junggar
Bortala
Karamay
Kuytun
Shihezi
Fig.1B
Urumqi
Ili
9.57
Tianshan
Aksu
Kuqa
Bayingol
Tarim
0
100
200
400 km
80°E
82°E
84°E
86°E
88°E
46°N
44°N
42°N
40°N
Earthquake magnitude
> 6
5-6
4-5
< 3
Earthquake depth
0-15 Km
15-30 Km
> 30 Km
city
thrust scarp
anticline axis
10 mm/yr
GPS velocity (Yang et al., 2008)
Paleozoic range limit

Figure 1

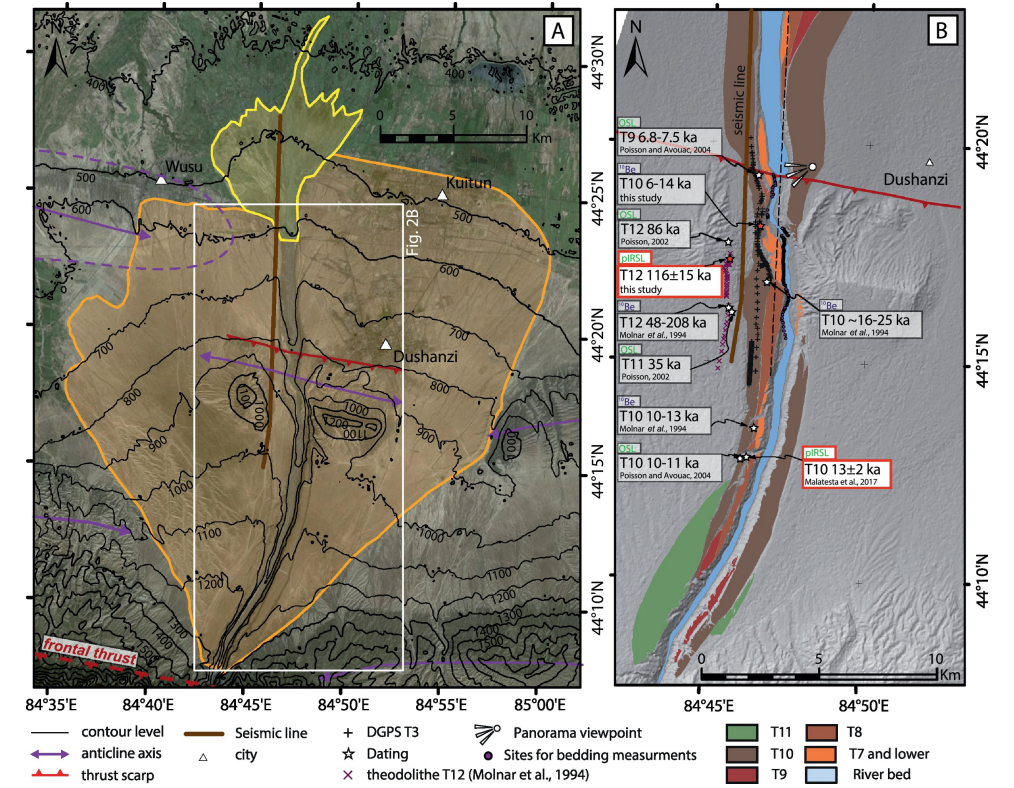
A
B
Wusu
Kuitun
Dushanzi
Fig. 2B
frontal thrust
0 5 10 Km
N
seismic line
T9 6.8-7.5 ka
Poisson and Avouac, 2004
T10 6-14 ka
this study
T12 86 ka
Poisson, 2002
T12 116±15 ka
this study
T12 48-208 ka
Molnar et al., 1994
T10 ~16-25 ka
Molnar et al., 1994
T11 35 ka
Poisson, 2002
T10 10-13 ka
Molnar et al., 1994
T10 10-11 ka
Poisson and Avouac, 2004
T10 13±2 ka
Malatesta et al., 2017
84°35'E
84°40'E
84°45'E
84°50'E
84°55'E
85°00'E
44°30'N
44°25'N
44°20'N
44°15'N
44°10'N
contour level
anticline axis
thrust scarp
Seismic line
city
DGPS T3
Dating
theodolithe T12 (Molnar et al., 1994)
Panorama viewpoint
Sites for bedding measurments
T11
T10
T9
T8
T7 and lower
River bed

Figure 2

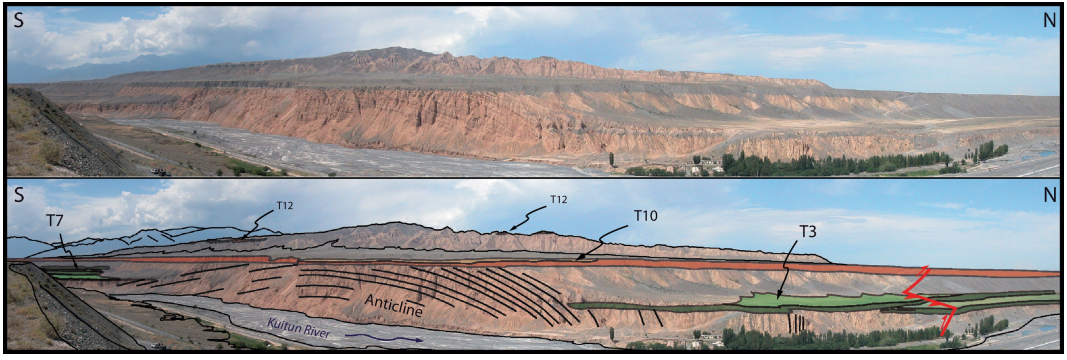

Figure 3

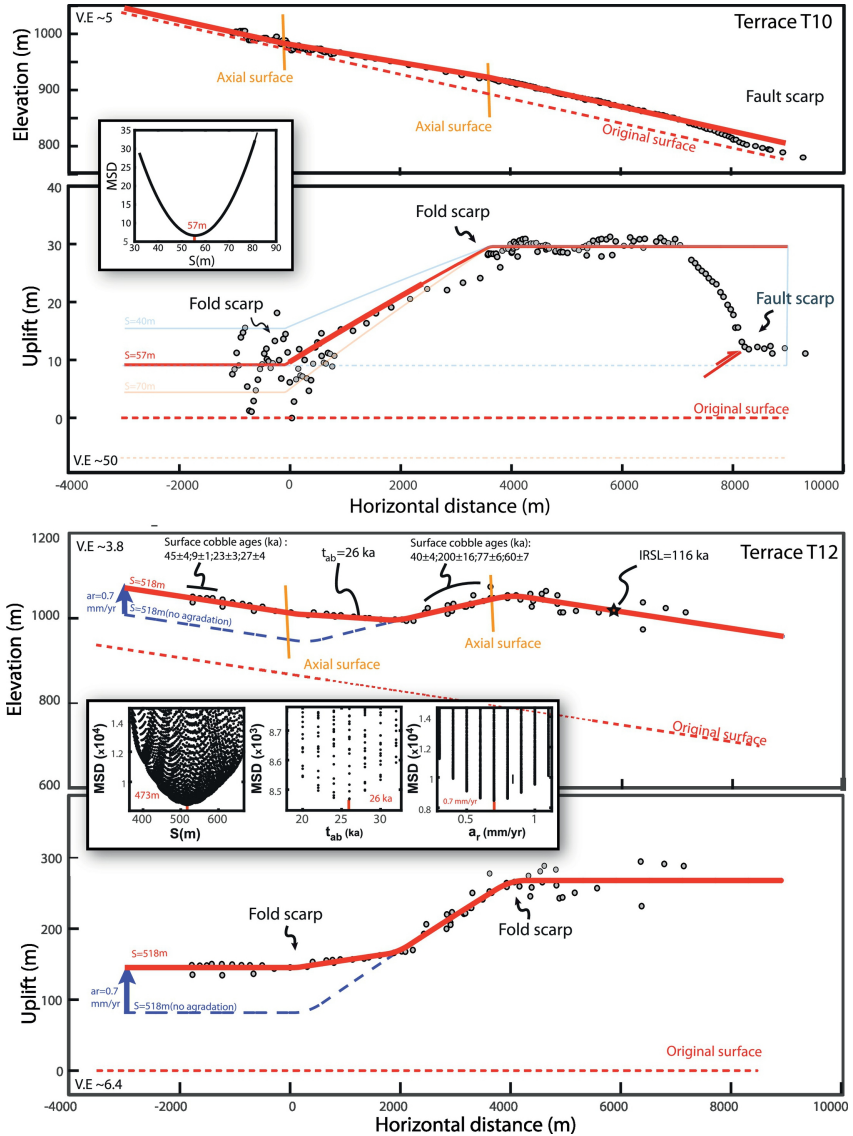
Terrace T10
V.E ~5
Elevation (m)
Axial surface
Axial surface
Fault scarp
Original surface
MSD
57m
S(m)
Fold scarp
Fold scarp
Fault scarp
S=40m
S=57m
S=70m
Original surface
Uplift (m)
V.E ~50
Horizontal distance (m)
Terrace T12
V.E ~3.8
Surface cobble ages (ka) :
45±4;9±1;23±3;27±4
t_ab=26 ka
Surface cobble ages (ka):
40±4;200±16;77±6;60±7
IRSL=116 ka
S=518m
ar=0.7
mm/yr
S=518m(no agradation)
Axial surface
Original surface
MSD (x10^4)
473m
S(m)
MSD (x10^3)
26 ka
t_ab (ka)
MSD (x10^4)
0.7 mm/yr
a_r (mm/yr)
Fold scarp
Fold scarp
S=518m
ar=0.7
mm/yr
S=518m(no agradation)
Original surface
Uplift (m)
V.E ~6.4
Horizontal distance (m)

Figure 4

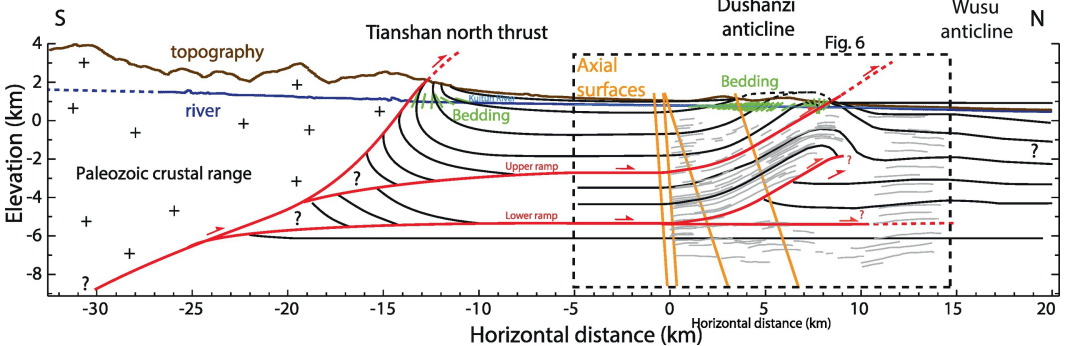
S
N
Tianshan north thrust
Dushanzi anticline
Wusu anticline
Fig. 6
topography
river
Paleozoic crustal range
Axial surfaces
Bedding
Bedding
Upper ramp
Lower ramp
Elevation (km)
Horizontal distance (km)
Horizontal distance (km)

Figure 5

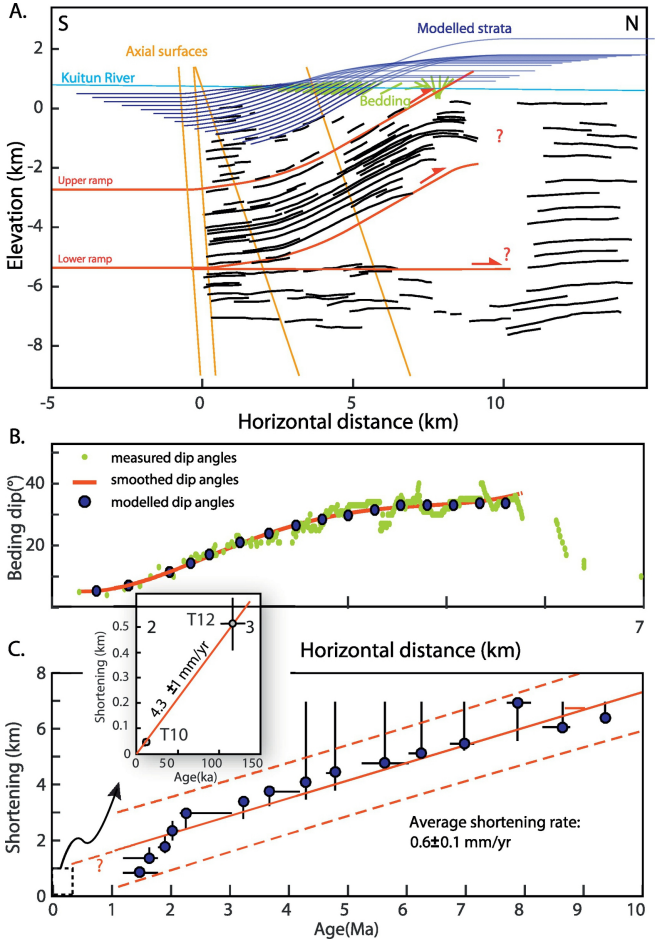
A.
S
N
Modelled strata
Axial surfaces
Kuitun River
Bedding
Upper ramp
Lower ramp
?
?
Elevation (km)
2
0
-2
-4
-6
-8
-5
0
5
10
Horizontal distance (km)
B.
measured dip angles
smoothed dip angles
modelled dip angles
Beding dip(°)
40
20
7
C.
Horizontal distance (km)
Shortening (km)
Age(Ma)
Average shortening rate:
0.6±0.1 mm/yr
?
T12
T10
2
3
4.3 ±1 mm/yr
Shortening (km)
Age(ka)
0.5
0.4
0.3
0.2
0.1
0
50
100
150

Figure 6